Ab initio study of geometrically metastable multiprotonated species: MH_n^{k+}

Alexander I. Boldyrev and Jack Simons
Department of Chemistry, The University of Utah, Salt Lake City, Utah 84112

(Received 24 April 1992; accepted 2 June 1992)

The geometries and stabilities relative to fragmentation of H_4O^{2+}, H_4S^{2+}, H_3F^{2+}, H_3Cl^{2+}, H_2Ne^{2+}, H_2Ar^{2+}; H_4F^{3+}, H_4Cl^{3+}, H_3Ne^{3+}, H_3Ar^{3+}; H_4Ne^{4+}, and H_4Ar^{4+} have been studied using the quadratic configuration interaction (with single and double excitations plus approximate triple excitations included) QCISD(T)/6–311G(2*df*,2*p*) method at second-order Møller–Plesset optimized geometries MP2(full)/TZP+ZPE/6–31G**. All of the triply charged H_4F^{3+}, H_4Cl^{3+}, H_3Ne^{3+}, and H_3Ar^{3+} and more highly charged H_4Ne^{4+} and H_4Ar^{4+} ions, as well as doubly charged H_2Ne^{2+} were not found to possess local minima on their zero-point corrected ground state surfaces, although H_4Cl^{3+} is only slightly unstable. Tetrahedral (T_d) structures for H_4O^{2+} and H_4S^{2+}, planar triangular (D_{3h}) H_3F^{2+}, triangular pyramidal (C_{3v}) H_3Cl^{2+} and bent (C_{2v}) H_2Ar^{2+} were found to be local minima on the respective ground state surfaces. The latter five species lie above their respective ion-plus-ion dissociation products by 61, 91, 111, 67, and 116 kcal/mol, and have barriers to dissociation of 38, 20, 12, 34, and 5 kcal/mol (all energies being zero-point corrected). Such multiply charged cations store a great deal of energy, which may be released by the addition of a single *extra* electron to form the corresponding cation of one less charge.

I. INTRODUCTION

A. Background

It is well known in chemistry that protons can exothermically attach to molecules and even to rare gas atoms (see Ref. 1, and references therein). Olah and others[2,3] have implicated the H_4O^{2+} and H_4S^{2+} dications as intermediates in proton–deuterium exchange reactions of isotopomeric hydronium and hydrosulfonium ions in so-called "magic acid" $FSO_3D{\cdot}SbF_5$ and FSO_3H–SbF_5–SO_2. Although small multiply charged ions are ubiquitous in aqueous solution, they are rarely observed to be stable in the gas phase where solvation energies are absent and where they are believed to undergo destruction by Coulomb explosion.

Large multiprotonated molecules may be thermodynamically stable even in the gas phase *if* their internal Coulomb repulsion energy can be made small (e.g., when the protons are attached to parts of the molecule that are distant from one another). In small gas-phase multiprotonated molecules MH_n^{k+} with a single "central" nonhydrogen atom, the Coulomb repulsion is expected to be very large, as a result of which such species might not be expected to be thermodynamically stable. However, when a cation of charge k is formed in which there are n ($>k$) symmetry-equivalent bonds to the central atom, the k charges can be distributed over n atoms. The resultant internal Coulombic repulsion among *fractional* charges of magnitude $\sim k/n$ may thus be low enough to render such species metastable. In such a case, a local minimum on the potential energy surface will occur as will a barrier to dissociation. In this article, we present results of our *ab initio* study of such multiply protonated small molecules.

B. Earlier work on multiply protonated systems

The thermodynamic stabilities of H_2Ne^{2+}, H_3F^{2+}, H_4O^{2+}, H_3Ne^{3+}, H_4F^{3+}, and H_4Ne^{4+} to loss of one proton have been studied at the self-consistent field (SCF) level with double-zeta basis sets (SCF/DZ) by Kozmuta *et al.*,[4] who found all of these multiprotonated species to be thermodynamically unstable to loss of a proton. Tetrahedral H_4O^{2+}, H_4F^{3+}, H_4S^{2+}, and H_4Cl^{3+} were optimized at the SCF level using a 6–31* basis set by Choi *et al.*[5] For H_4O^{2+} and H_4S^{2+}, *ab initio* calculations of the vibrational frequencies and of the energy barriers to dissociation were carried out at the SCF/6–31G* level in Refs. 2 and 3. The H_4O^{2+} dication was found to be thermodynamically unstable by 59.2 kcal/mol, but its tetrahedral structure was identified[2] as a local minimum with a dissociation barrier of 39.4 kcal/mol. The H_4S^{2+} dication was also found[3] to be thermodynamically unstable (by 27.2 kcal/mol), with the tetrahedral structure being a local minimum with a dissociation barrier of 57.3 kcal/mol. These thermodynamic energies and barriers were found to not change significantly when electron correlation corrections were included. Specifically, at the SCF/6–31G*-optimized geometries using fourth-order Møller–Plesset perturbation theory (MP4SDTQ/6–31G**) the exothermicities and barriers were 43.9 and 52.9 kcal/mol for H_4O^{2+} and 25.2 and 59.2 kcal/mol for H_4S^{2+}.

C. This work

In this study, we reexamined these species using more flexible basis sets and more systematic treatments of electron correlation. As a result of this study, we predict that several of these dications are metastable species which have reasonably high barriers to dissociation. These properties of the corresponding potential energy surfaces may make materials containing these cations interesting candidates for use in energy storage. As illustrated in Sec. III, the pent up energy of these species may be released by adding an extra electron (e.g., electrochemically or via photoinduced

 0021-9606/92/184272-10$006.00

charge transfer from a neighboring counter ion) to form the species with one lower positive charge.

II. COMPUTATIONAL DETAILS

The geometries of HNe^+, H_2Ne^{2+}, H_3Ne^{3+}, H_4Ne^{4+}, HF, H_2F^+, H_3F^{2+}, H_4F^{3+}, H_2O, H_3O^+, H_4O^{2+}, HAr^+, H_2Ar^{2+}, H_3Ar^{3+}, H_4Ar^{4+}, HCl, H_2Cl^+, H_3Cl^{2+}, H_4Cl^{3+}, H_2S, H_3S^+, and H_4S^{2+} were first optimized employing analytical SCF gradients[6] with a polarized split-valence basis set [results at this level are denoted SCF/6–31G** (Refs. 7–9)] and at the correlated MP2(full) level. The final optimized geometries were obtained using MP2(full) calculations with the triple-zeta plus polarization basis (TZP) of Huzinaga and Dunning $(10s6p/5s3p)+3d$ functions ($\alpha_d = 0.88$ for O and 0.95 for F) for O and F (Ref. 9) and the McLean–Chandler $(12s9p/6s5p)+3d$ functions [$\alpha_d = 0.65$ for S, 0.75 for Cl, and 0.85 for Ar (Ref. 10)]. The fundamental vibrational frequencies, normal coordinates, and zero-point energies (ZPE) were calculated by standard FG matrix methods. Finally, correlated total energies were evaluated in the full fourth-order frozen-core approximation both by Møller–Plesset perturbation theory[11] (MP4) and by the quadratic configuration interaction including singles and doubles with approximate triples QCISD(T)[12] method using the 6–311G(2*df*,2*p*) standard basis sets. The GAUSSIAN 90 program suite[13] was used to perform all of the calculations whose results are discussed here.

III. RESULTS AND DISCUSSION

Our calculated geometries (Table I), total energies at various levels of theory (Tables II and III), dissociation energies and barriers (Table IV), harmonic vibrational frequencies as well as infrared (ir) and Raman intensities and zero-point energies (ZPE) (Tables V) are given in Tables I–V. The calculated geometries of H_2O, H_3O^+, H_2S,

TABLE I. Calculated and experimental geometries (Å and degrees).

Species	Symmetry	Method	R(M–H)	HMH, angle
$H_2O,{}^1A_1$	C_{2v}	SCF/6–31G**	0.943	106.0
		MP2(full)/6–31G**	0.961	103.9
		MP2(full)/TZP	0.962	105.1
		EXPT[c]	0.957	104.5
$H_3O^+,{}^1A_1$	C_{3v}	SCF/6–31G**	0.961	114.7
		MP2(full)/6–31G**	0.979	112.6
		MP2(full)/TZP	0.980	112.6
$H_4O^{2+},{}^1A_1$	T_d	SCF/6–31G**	1.023	109.47
		MP2(full)/6–31G**	1.043	109.47
		MP2(full)/TZP	1.044	109.47
H_4O^{2+}(ts),$^1A_1$	C_{3v}	SCF/6–31G**	2.064[a]	
			0.985[b]	110.9[c]
		MP2(full)/6–31G**	2.158[a]	
			1.004[b]	111.5[c]
		MP2(full)/TZP	2.144[a]	
			1.006[b]	111.6[c]
$H_2S,{}^1A_1$	C_{2v}	SCF/6–31G**	1.327	94.4
		MP2(full)/6–31G**	1.329	92.8
		MP2(full)/TZP	1.333	92.1
		EXPT	1.336	92.06
$H_3S^+,{}^1A_1$	C_{3v}	SCF/6–31G**	1.335	97.1
		MP2(full)/6–31G**	1.339	95.8
		MP2(full)/TZP	1.346	94.9
$H_3S^+,{}^1A_1'$	D_{3h}	SCF/6–31G**	1.322	120.
		MP2(full)/6–31G**	1.324	120.
		MP2(full)/TZP	1.330	120.
$H_4S^{2+},{}^1A_1$	T_d	SCF/6–31G**	1.360	109.47
		MP2(full)/6–31G**	1.366	109.47
		MP2(full)/TZP	1.378	109.47
H_4S^{2+}(ts),$^1A_1$	C_{3v}	SCF/6–31G**	2.772[a]	
			1.344[b]	117.1[c]
		MP2(full)/6–31G**	2.822[a]	
			1.349[b]	117.8[c]
		MP2(full)/TZP	2.830[a]	
			1.357[b]	118.2[c]
$HF,{}^1\Sigma^+$	$C_{\infty v}$	SCF/6–31G**	0.901	
		MP2(full)/6–31G**	0.921	
		MP2(full)/TZP	0.925	
		EXPT	0.917	
$H_2F^+,{}^1A_1$	C_{2v}	SCF/6–31G**	0.944	115.9
		MP2(full)/6–31G**	0.966	112.7

TABLE I. (*Continued.*)

Species	Symmetry	Method	R(M–H)	HMH, angle
		MP2(full)/TZP	0.968	113.0
$H_3F^{2+},{}^1A_1'$	D_{3h}	SCF/6–31G**	1.047	120.
		MP2(full)/6–31G**	1.073	120.
		MP2(full)/TZP	1.071	120.
H_3F^{2+}(ts),$^1A_1$	C_{2v}	SCF/6–31G**	1.581[a]	
			0.995[b]	113.7[c]
		MP2(full)/6–31G**	1.639[a]	
			1.018[b]	112.5[c]
		MP2(full)/TZP	1.648[a]	
			1.021[b]	115.5[c]
$HCl,{}^1\Sigma^+$	$C_{\infty v}$	SCF/6–31G**	1.266	
		MP2(full)/6–31G**	1.268	
		MP2(full)/TZP	1.274	
		EXPT	1.275	
$H_2Cl^+,{}^1A_1$	C_{2v}	SCF/6–31G**	1.290	97.3
		MP2(full)/6–31G**	1.293	95.9
		MP2(full)/TZP	1.300	94.2
$H_3Cl^{2+},{}^1A_1$	C_{3v}	SCF/6–31G**	1.348	100.7
		MP2(full)/6–31G**	1.353	95.8
		MP2(full)/TZP	1.365	98.4
$H_3Cl^{2+},{}^1A_1'$	D_{3h}	SCF/6–31G**	1.358	120.
		MP2(full)/6–31G**	1.360	120.
		MP2(full)/TZP	1.373	120.
H_3Cl^{2+}(ts),$^1A_1$	C_s	SCF/6–31G**	2.336[a]	109.6[b]
			1.315[c]	98.8[d]
		MP2(full)/6–31G**	2.432[a]	108.4[b]
			1.319[c]	97.4[d]
		MP2(full)/TZP	2.471[a]	108.8[b]
			1.326[c]	95.9[d]
$H_4Cl^{3+},{}^1A_1$	T_d	SCF/6–31G**	1.493	109.47
		MP2(full)/6–31G**	1.500	109.47
		MP2(full)/TZP	1.521	109.47
$HNe^+,{}^1\Sigma^+$	$C_{\infty v}$	SCF/6–31G**	0.985	
		MP2(full)/6–31G**	1.007	
$HAr^+,{}^1\Sigma^+$	$C_{\infty v}$	SCF/6–31G**	1.267	
		MP2(full)/6–31G**	1.268	
		MP2(full)/TZP	1.278	
$H_2Ar^{2+},{}^1A_1$	C_{2v}	SCF/6–31G**	1.389	104.9
		MP2(full)/6–31G**	1.385	103.7
		MP2(full)/TZP	1.4051	102.5
H_2Ar^{2+}(ts),$^1A'$	C_s	SCF/6–31G**	1.863[a]	
			1.340[b]	111.9[c]
		MP2(full)/6–31G**	1.910[a]	
			1.334[b]	110.9[c]
		MP2(full)/TZP	1.998[a]	
			1.343[b]	111.5[c]

[a]The distance between the central atom and the departing H atom labled *b*.
[b]The distance between the central atom and the other H atoms labled *t*.
[c]The angle H_bMH_t.
[d]The angle H_tMH_t.
[e]Data taken from M. W. Chase, Jr., C. A. Davies, J. R. Downey, Jr., D. J. Fouip, R. A. McDonald, A. N. Syverud, *JANAF Thermochemical Tables*, 3rd ed., J. Phys. Chem. Ref. Data **14** (1985), Suppl. 1.

H_3S^+, HF, NeH^+, ArH^+, and HCl as well as the dissociation energies of the H_3O^+, H_3S^+, H_2F^+, HNe^+, HAr^+, and H_2Cl^+ cations are in good agreement ($\leqslant$3 kcal/mol for the energies) with experimental data. We expect our results to be equally accurate for the doubly and triply charged species (for which experimental data are not available). Now, let us focus on each of the various classes of multiply protonated cations treated here, in each case considering the species' geometries, vibrational frequencies, ir intensities, and energetic stabilities.

A. H_4O^{2+} and H_4S^{2+}

1. Nature of the $H_4O^{2+} \rightarrow H_3O^+ + H^+$ energy surface

Both of the above dications have tetrahedral local-minimum structures as expected. The potential energy sur

TABLE II. Calculated total energies E_{TOT} (a.u.) of the OH_n^{k+}, FH_n^{k+}, NeH_n^{k+}, SH_n^{k+}, ClH_n^{k+}, and ArH_n^{k+} cations.

Species	Symmetry	State	SCF/6–31G**	MP2(full)/6–31G**	MP2(full)6–311G**[a]
OH_2	C_{2v}	$^1A_1$	−76.023 62	−76.222 45	−76.287 13
OH_3^+	C_{3v}	$^1A_1$	−76.310 32	−76.508 97	−76.564 09
OH_4^{2+}	T_d	$^1A_1$	−76.220 63	−76.424 51	−76.479 91
OH_4^{2+}(ts)	C_{3v}	$^1A_1$	−76.151 26	−76.355 28	−76.409 78
FH	$C_{\infty v}$	$^1\Sigma^+$	−100.011 69	−100.196 70	−100.289 15
FH_2^+	C_{2v}	$^1A_1$	−100.215 18	−100.404 30	−100.483 03
FH_3^{2+}	D_{3h}	$^1A_1'$	−100.041 87	−100.235 89	−100.313 12
FH_3^{2+}(ts)	C_{2v}	$^1A_1$	−100.025 86	−100.219 33	−100.288 85
FH_4^{3+}	T_d	$^1A_1$	−99.580 64	−99.790 48	−99.864 40
Ne		^1S	−128.474 41	−128.626 18	
NeH^+	$C_{\infty v}$	$^1\Sigma^+$	−128.555 88	−128.716 72	
SH_2	C_{2v}	$^1A_1$	−398.675 03	−398.821 13	−398.967 13
SH_3^+	C_{3v}	$^1A_1$	−398.952 53	−399.102 97	−399.250 56
SH_3^+	D_{3h}	$^1A_1'$	−398.903 34	−399.054 00	−399.200 18
SH_4^{2+}	T_d	$^1A_1$	−398.914 48	−399.063 14	−399.212 69
SH_4^{2+}(ts)	C_{3v}	$^1A_1$	−398.818 47	−398.969 60	−399.115 96
ClH	$C_{\infty v}$	$^1\Sigma^+$	−460.066 21	−460.215 62	−460.292 97
ClH_2^+	C_{2v}	$^1A_1$	−460.278 83	−460.436 39	−460.516 25
ClH_3^{2+}	C_{3v}	$^1A_1$	−460.175 37	−460.336 64	−460.420 09
ClH_3^{2+}	D_{3h}	$^1A_1'$	−460.147 15	−460.307 20	−460.389 36
ClH_3^{2+}(ts)	C_s	$^1A'$	−460.128 69	−460.281 11	−460.360 03
ClH_4^{3+}	T_d	$^1A_1$	−459.791 47	−459.952 78	−460.041 98
ClH_4^{3+}(ts_1)	C_{3v}	$^1A_1$	−459.790 56	−459.951 85	−460.041 11
ClH_4^{3+}(ts_2)	C_{2v}	$^1A_1$	−459.786 51	−459.947 98	
Ar		^1S	−526.773 75	−526.919 99	−527.007 48
ArH^+	$C_{\infty v}$	$^1\Sigma^+$	−526.909 61	−527.066 87	−527.158 81
ArH_2^{2+}	C_{2v}	$^1A_1$	−526.719 41	−526.881 81	−526.978 68
ArH_2^{2+}(ts)	C_s	$^1A'$	−526.709 34	−526.869 06	−526.964 68

[a]For the OH_n^{k+} and FH_n^{k+} species, (10*s*6*p*1*d*/5*s*3*p*1) basis sets were used for O and F and a (5*s*1*p*/3*s*1*p*) basis set was used for H.

TABLE III. Calculated correlated energies (a.u.) of the OH_n^{k+}, FH_n^{k+}, NeH_n^{k+}, SH_n^{k+}, ClH_n^{k+}, and ArH_n^{k+} cations.

Species	Symmetry	State	MP2/6–311G (2*df*, 2*p*)	MP3/6–311G (2*df*, 2*p*)	MP4/6–311G (2*df*, 2*p*)	QCISD(T) /6–311G(2*df*, 2*p*)
Ne		^1S	−128.779 69	−128.781 49	−128.786 67	−128.786 27
NeH^+	$C_{\infty v}$	$^1\Sigma^+$	−128.867 65	−128.868 70	−128.875 72	−128.875 09
FH	$C_{\infty v}$	$^1\Sigma^+$	−100.314 45	−100.315 74	−100.324 22	−100.323 56
FH_2^+	C_{2v}	$^1A_1$	−100.514 36	−100.516 48	−100.525 22	−100.524 65
FH_3^{2+}	D_{3h}	$^1A_1'$	−100.340 82	−100.341 95	−100.351 12	−100.350 46
FH_3^{2+}(ts)	C_{2v}	$^1A_1$	−100.319 16	−100.318 65	−100.329 16	−100.328 14
FH_4^{3+}	T_d	$^1A_1$	−99.891 56	−99.883 69	−99.899 56	−99.896 82
OH_2	C_{2v}	$^1A_1$	−76.305 22	−76.310 38	−76.319 83	−76.319 38
OH_3^+	C_{3v}	$^1A_1$	−76.584 99	−76.592 22	−76.600 74	−76.600 58
OH_4^{2+}	T_d	$^1A_1$	−76.495 99	−76.502 86	−76.511 70	−76.511 65
OH_4^{2+}(ts)	C_{3v}	$^1A_1$	−76.429 45	−76.434 60	−76.444 48	−76.444 07
Ar		^1S	−526.976 42	−526.990 34	−526.992 66	−526.992 77
ArH^+	$C_{\infty v}$	$^1\Sigma^+$	−527.122 23	−527.138 45	−527.142 33	−527.142 78
ArH_2^{2+}	C_{2v}	$^1A_1$	−526.940 35	−526.957 21	−526.961 86	−526.962 59
ArH_2^{2+}(ts)	C_s	$^1A'$	−526.930 71	−526.946 45	−526.950 75	−526.951 30
ClH	$C_{\infty v}$	$^1\Sigma^+$	−460.293 74	−460.314 18	−460.320 86	−460.321 34
ClH_2^+	C_{2v}	$^1A_1$	−460.510 43	−460.532 97	−460.540 28	−460.541 13
ClH_3^{2+}	C_{3v}	$^1A_1$	−460.409 81	−460.433 14	−460.440 77	−460.441 93
ClH_3^{2+}	D_{3h}	$^1A_1'$	−460.378 10	−460.401 09	−460.408 36	−460.409 28
ClH_3^{2+}(ts)	C_s	$^1A'$	−460.355 06	−460.376 67	−460.384 32	−460.385 11
ClH_4^{3+}	T_d	$^1A_1$	−460.027 93	−460.050 28	−460.057 87	−460.058 90
ClH_4^{3+}(ts_1)	C_{3v}	$^1A_1$	−460.028 08	−460.050 26	−460.057 85	−460.058 85
SH_2	C_{2v}	$^1A_1$	−398.888 74	−398.911 71	−398.919 44	−398.920 43
SH_3^+	C_{3v}	$^1A_1$	−399.165 07	−399.189 80	−399.197 83	−399.199 36
SH_3^+	D_{3h}	$^1A_1'$	−399.115 62	−399.139 97	−399.147 54	−399.148 74
SH_4^{2+}	T_d	$^1A_1$	−399.029 34	−399.052 91	−399.061 09	−399.062 39
SH_4^{2+}(ts)	C_{3v}	$^1A_1$	−398.995 25	−399.015 26	399.021 74	−399.023 15

[a]Total energies of the NeH^+ cation calculated at the MP2(full)/6–31G** geometry. For Ar, ArH^+, and ArH_2^{2+} a 311G(2*d*,2*p*) basis set was employed.

TABLE IV. Calculated dissociation energies (E_{diss}) and dissociation barriers (E^+) (kcal/mol) at MP2(full)/6–311G** geometries With the 6–311G(2*df*,2*p*)[a] basis sets.

Reaction	MP2		MP3		MP4		QCISD(T)		QCISD(T)+ZPE[b]	
	E_{diss}	E^+	E_{diss}	E^+	E_{diss}	E^+	E_{diss}	E^+	E_{diss}	E^+
1. OH_3^+–OH_2+H^+	+175.6	···	+176.9	···	+176.3	···	+176.5	···	+168.0	···
2. OH_4^{2+}–OH_2+$2H^+$	+119.7	···	+120.8	···	+120.4	···	+120.7	···	+106.7	···
3. OH_4^{2+}–OH_3^++H^+	−55.8	41.8	−56.1	42.8	−55.9	42.2	−55.8	42.4	−61.3	38.1
4. FH_2^+–FH+H^+	+125.4	···	+126.0	···	+126.1	···	+126.2		+120.0	
5. FH_3^{2+}–FH+$2H^+$	+16.5	···	+16.4	···	+16.9	···	+16.9	···	+8.9	···
6. FH_3^{2+}–FH_2^++H^+	−108.9	13.6	−109.5	14.6	−109.2	13.8	−109.3	14.0	−111.1	12.2
7. FH_4^{2+}–FH+$3H^+$	−265.4	···	−271.1	···	−266.5	···	−267.8	···	−270.8	···
8. FH_4^{3+}–FH_2^++$2H^+$	−390.8	···	−397.1	···	−392.6	···	−394.0	···	−390.8	···
9. FH_4^{3+}–FH_3^{2+}+H^+	−281.9	···	−287.6	···	−283.4	···	−284.7	···	−279.7	···
10. NeH^+–Ne+H^+	+55.2	···	+54.7	···	+55.9	···	+55.7	···	+51.7	···
11. SH_3^+–SH_2+H^+	+173.4	···	+174.5	···	+174.7	···	+175.0	···	+167.8	···
12. SH_4^{2+}–SH_2+$2H^+$	+88.2	···	+88.6	···	+88.9	···	+89.1	···	+76.4	···
13. SH_4^{2+}–SH_3^++H^+	−85.2	21.4	−85.9	23.6	−85.8	24.7	−85.9	24.6	−91.4	19.7
14. ClH_2^+–ClH+H^+	+136.0	···	+137.3	···	+137.7	···	+137.9	···	+132.2	···
15. ClH_3^{2+}–ClH+$2H^+$	+72.8	···	+74.6	···	+75.2	···	+75.7	···	+65.0	···
16. ClH_3^{2+}–ClH_2^++H^+	−63.1	34.4	−62.6	35.4	−62.4	35.4	−62.2	35.7	−67.2	33.8
17. ClH_4^{3+}–ClH+$3H^+$	−166.8	···	−165.6	···	−165.0	···	−164.7	···	−173.7	···
18. ClH_4^{3+}–ClH_2^++$2H^+$	−302.8	···	−302.9	···	−302.7	···	−302.6	···	−305.9	···
19. ClH_4^{3+}–ClH_3^{2+}+H^+	−239.6	−0.1	−240.2	0.0	−240.3	0.0	−240.4	0.0	−242.9	0.0
20. ArH^+–Ar+H	+91.5	···	+92.9	···	+93.9	···	+94.1	···	+90.0	···
21. ArH_2^{2+}–Ar+$2H^+$	−22.6	···	−20.8	···	−19.3	···	−18.9	···	−25.7	···
22. ArH_2^{2+}–ArH^++H^+	−114.1	6.0	−113.7	6.8	−113.2	7.0	−113.1	7.1	−115.8	4.6

[a]The argon containing species were calculated with a 6–311G(2*d*,2*p*) basis set.
[b]Zero-point corrected.

TABLE V. (a) Calculated frequencies (cm^{-1}) and ir (KM/mol) and Raman ($Å^4$/amu) intensities of OH_n^{k+} species. (b) Calculated frequencies (cm^{-1}) and ir (KM/mol) and Raman ($Å^4$/amu) intensities of FH_n^{k+} and NeH^+ species. (c) Calculated frequencies (cm^{-1}) and ir (KM/mol) and Raman ($Å^4$/amu) intensities of SH_n^{k+} speicies. (d) Calculated frequencies (cm^{-1}) and ir (KM/mol) and Raman ($Å^4$/amu) intensities of ClH_n^{k+} and ArH_n^{k+} species.

(a)	Species	Symmetry	State	SCF/6–31G** Freq.	*MP*2(full)/6–31G** ir	Ram.	Freq.	Exptl. ir	Freq.[a]
	OH_2	C_{2v}	$^1A_1$	$\nu_1(a_1)$ = 4147	16	75	3895	4	3656.65
				$\nu_2(a_1)$ = 1770	105	6	1683	78	1594.78
				$\nu_3(b_2)$ = 4264	58	37	4033	34	3755.79
				ZPE=14.6			13.7		
	OH_3^+	C_{3v}	$^1A_1$	$\nu_1(a_1)$ = 3857	46	39	3644	47	
				$\nu_2(a_1)$ = 782	629	1	867	547	
				$\nu_3(e)$ = 3993	630	11	3785	522	
				$\nu_4(e)$ = 1789	141	2	1712	121	
				ZPE=23.2			22.2		
	OH_4^{2+}	T_d	$^1A_1$	$\nu_1(a_1)$ = 3175	0	30	2967	0	
				$\nu_2(e)$ = 1702	0	3	1631	0	
				$\nu_3(t_2)$ = 3069	1164	7	2893	1049	
				$\nu_4(t_2)$ = 1569	438	1	1480	414	
				ZPE=29.3			27.7		
	OH_4^{2+}(ts)	C_{3v}	$^1A_1$	$\nu_1(a_1)$ = 3576			3355		
				$\nu_2(a_1)$ = 1421			1341		
				$\nu_3(a_1)$ = 872*i*			837*i*		
				$\nu_4(e)$ = 3615			3423		
				$\nu_5(e)$ = 1773			1688		
				$\nu_6(e)$ = 787			732		
				ZPE=24.8			23.4		

(b)	Species	Symmetry	State	SCF/6–31G** Freq.	ir	Ram.	*MP*2(full)/6–31G** Freq.	ir	Exptl. Freq.[a]
	FH	$C_{\infty v}$	$^1\Sigma^+$	ωe=4493	133	30	4193	82	4141.03
				ZPE=6.4			6.0		
	FH_2^+	C_{2v}	$^1A_1$	$\nu_1(a_1)$ = 3796	290	18	3539	242	
				$\nu_2(a_1)$ = 1481	329	1	1453	287	
				$\nu_3(b_2)$ = 3800	1062	5	3569	881	
				ZPE=13.0			12.2		

TABLE V. (*Continued.*)

(b)	Species	Symmetry	State	SCF/6–31G** Freq.	ir	Ram.	*MP2*(full)/6–31G** Freq.	ir	Exptl. Freq.[a]
	FH_3^{2+}	D_{3h}	$^1A_1'$	$\nu_1(a_1')$ = 2615	0	13	2757	0	
				$\nu_2(a_2'')$ = 574	1175	0	396	1140	
				$\nu_3(e')$ = 2253	2183	1	2140	2064	
				$\nu_4(e')$ = 1406	172	1	1330	159	
				ZPE=15.0			14.0		
	FH_3^{2+}(ts)	C_{2v}	$^1A_1$	$\nu_1(a_1)$ = 3105			2917		
				$\nu_2(a_1)$ = 1550			1485		
				$\nu_3(a_1)$ = 1069*i*			1031*i*		
				$\nu_4(b_1)$ = 587			462		
				$\nu_5(b_2)$ = 2981			2829		
				$\nu_6(b_2)$ = 906			849		
				ZPE=13.1			12.2		
	FH_4^{3+}	T_d	$^1A_1$	$\nu_1(a_1)$ = 1210			1181		
				$\nu_2(e)$ = 993			977		
				$\nu_3(t_2)$ = 1102			1043		
				$\nu_4(t_2)$ = 1396*i*			1266*i*		
				ZPE=9.3			9.0		
	NeH^+	$C_{\infty v}$	$^1\Sigma^+$	ν=2884			2805		
				ZPE=4.1			4.0		

(c)	Species	Symmetry	State	SCF/6–31G** Freq.	ir	Ram.	MP2(full)/6–31G** Freq.	ir	Exptl. Freq.[a]
	SH_2	C_{2v}	$^1A_1$	$\nu_1(a_1)$ = 2897	4	178	2847	4	2614.56
				$\nu_2(a_1)$ = 1341	7	44	1270	8	1182.68
				$\nu_3(b_2)$ = 2909	8	134	2874	7	2625
				ZPE=10.2			10.0		
	SH_3^+	C_{3v}	$^1A_1$	$\nu_1(a_1)$ = 2850	50	158	2777	48	
				$\nu_2(a_1)$ = 1169	12	12	1119	11	
				$\nu_3(e)$ = 2860	79	87	2800	74	
				$\nu_4(e)$ = 1367	0	31	1283	0	
				ZPE=17.8			17.2		
	SH_3^+	D_{3h}	$^1A_1'$	$\nu_1(a_1)$ = 2870			2827		
				$\nu_2(a_2'')$ = 1191*i*			1139*i*		
				$\nu_3(e')$ = 2965			2928		
				$\nu_4(e')$ = 1206			1143		
				ZPE=16.0			15.7		
	SH_4^{2+}	T_d	$^1A_1$	$\nu_1(a_1)$ = 2631	0	168	2557	0	
				$\nu_2(e)$ = 1315	0	22	1243	0	
				$\nu_3(t_2)$ = 2640	596	39	2574	587	
				$\nu_4(t_2)$ = 1101	24	6	1026	31	
				ZPE=23.6			22.7		
	SH_4^{2+}(ts)	C_{3v}	$^1A_1$	$\nu_1(a_1)$ = 2759			2687		
				$\nu_2(a_1)$ = 1098			1049		
				$\nu_3(a_1)$ = 715*i*			716*i*		
				$\nu_4(e)$ = 2772			2710		
				$\nu_5(e)$ = 1315			1240		
				$\nu_6(e)$ = 429			402		
				ZPE=1-8.4			17.8		

(d)	Species	Symmetry	State	SCF/6–31G** Freq.	ir	Ram.	MP2(full)/6–31G** Freq.	ir	Exptl. Freq.[a]
	ClH	$C_{\infty v}$	$^1\Sigma^+$	ω_e=3180	34	117	3125	22	2990.94
				ZPE=4.5			4.5		
	ClH_2^+	C_{2v}	$^1A_1$	$\nu_1(a_1)$ = 2967	233	96	2909	197	
				$\nu_2(a_1)$ = 1351	21	19	1277	18	
				$\nu_3(b_2)$ = 2962	362	57	2916	300	
				ZPE=10.4			10.2		
	ClH_3^{2+}	C_{3v}	$^1A_1$	$\nu_1(a_1)$ = 2509	409	87	2453	372	
				$\nu_2(a_1)$ = 1035	192	7	1009	178	
				$\nu_3(e)$ = 2410	1003	34	2367	880	
				$\nu_4(e)$ = 1286	28	15	1220	28	
				ZPE=15.6			15.2		
	ClH_3^{2+}	D_{3h}	$^1A_1'$	$\nu_1(a_1')$ = 2365			2347		
				$\nu_2(a_2'')$ = 925*i*			915*i*		
				$\nu_3(e')$ = 2313			2306		

TABLE V. (*Continued.*)

(d)	Species	Symmetry	State	SCF/6–31G** Freq.	ir	Ram.	MP2(full)/6–31G** Freq.	ir	Exptl. Freq.[a]
				$\nu_4(e') = 1088$			1035		
				ZPE=13.1			12.9		
	ClH_3^{2+}(ts)	C_s	$^1A'$	$\nu_1(a') = 2735$			2683		
				$\nu_2(a') = 1302$			1237		
				$\nu_3(a') = 554$			523		
				$\nu_4(a') = 841i$			817i		
				$\nu_5(a'') = 2713$			2675		
				$\nu_6(a'') = 616$			588		
				ZPE=11.3			11.0		
	ClH_4^{3+}	T_d	$^1A_1$	$\nu_1(a_1) = 1612$	0	90	1591	0	
				$\nu_2(e) = 1062$	0	17	1012	0	
				$\nu_3(t_2) = 1237$	2673	7	1220	2531	
				$\nu_4(t_2) = 764$	14	11	727	2	
				ZPE=13.9			13.5		
	ClH_4^{3+}(ts_1)	C_{3v}	$^1A_1$	$\nu_1(a_1) = 1713$			1691		
				$\nu_2(a_1) = 950$			907		
				$\nu_3(a_1) = 895i$			888i		
				$\nu_4(e) = 1441$			1426		
				$\nu_5(e) = 1062$			1012		
				$\nu_6(e) = 750$			712		
				ZPE=13.1			12.7		
	ClH_4^{3+}(ts_2)	C_{2v}	$^1A_1$	$\nu_1(a_1) = 1965$			1947		
				$\nu_2(a_1) = 1125$			1074		
				$\nu_3(a_1) = 671$			639		
				$\nu_4(a_1) = 857i$			844i		
				$\nu_5(a_2) = 936$			896		
				$\nu_6(b_1) = 1837$			1828		
				$\nu_7(b_1) = 697$			666		
				$\nu_8(b_2) = 874$			837		
				$\nu_9(b_2) = 1243i$			1244i		
				ZPE=11.6			11.3		
	ArH^+	$C_{\infty v}$	$^1\Sigma^+$	ν=2896	680	43	2884	567	
				ZPE=4.1			4.1		
	ArH_2^{2+}	C_{2v}	$^1A_1$	$\nu_1(a_1) = 1953$	1003	34	1989	882	
				$\nu_2(a_1) = 1040$	127	9	1024	128	
				$\nu_3(b_2) = 1699$	1976	13	1766	1747	
				ZPE=6.7			6.8		
	ArH_2^{2+}(ts)	C_s	$^1A'$	$\nu_1(a') = 2230$			2282		
				$\nu_2(a') = 736$			710		
				$\nu_3(a') = 1041i$			1033i		
				ZPE=4.2			4.3		

[a]Data from M. W. Chase, Jr., C. A. Davies, J. R. Downey, Jr., D. J. Fouip, R. A. McDonald, A. N. Syverud, *JANAF Thermochemical Tables*, 3rd ed. J. Phys. Chem. Ref. Data **14** (1985), Suppl. 1.

faces (see Fig. 1 for that of the oxygen-containing dication) for H_4O^{2+} and H_4S^{2+} are repulsive at large H_3X^+–H^+ separation due to the large Coulomb repulsion between the two unit positive charges. Near the barrier, electron density from the H_3X^+ moiety flows to the approaching H^+ ion, as the fourth X–H σ bond begins to form. This flow in density is monitored in Fig. 1 through the partial charges on the approaching (H_b) and three equivalent (H_t) hydrogen atom centers. Once this new bond is formed, the entire +2 charge is distributed through all *four* H atom centers as a result of which the quantum mechanical Coulomb repulsion energy is dramatically reduced. At the tetrahedral geometry, the charge delocalization is optimal and entirely uniform, and the total energy is a minimum.

2. Comparison with classical Coulomb electrostatic energies

It is informative to examine the nature of the Coulombic energy content of these species in further detail, and, in particular, to compare the results of our quantum calculations to predictions of various classical electrostatic models. So doing can increase our understanding of the forces that act to stabilize these species.

In Fig. 1 we display our fully quantal H_4O^{2+} energies as functions of the distance R(OH) between the O atom and the unique H^+ cation [with the other internal geometrical degrees of freedom optimized for each such R(OH)]. Also shown are the corresponding energies (at these same nuclear geometries) of a classical model that intentionally excludes bond formation with the approaching H^+ ion.

The higher energy curve in Fig. 1 gives the energy of interaction of a unit positive charge located on the unique H center with an H_3O^+ ion whose internal geometry is made identical to that obtained in our *ab initio* H_4O^{2+} calculations at each R(OH), but whose orbitals have been SCF-optimized in the presence of the unit positive charge on the unique H center. In these calculations, the net charges on the three identical H atoms and the O atom reflect the quantal charge distribution of H_3O^+ polarized by the unit positive charge at R(OH). Although these energies closely parallel the correct H_4O^{2+} energies down to $\sim$2.1 Å, they deviate strongly for shorter distances. In particular, as the fourth O–H bond begins to form, the H_4O^{2+} quantum energy (which contains an attractive O–H bond energy contribution that both classical curves are lacking) drops significantly below this energy. For example, at the H_4O^{2+} equilibrium geometry, the quantum energy is 56 kcal/mol above the $H_3O^+ + H^+$ asymptote whereas this model's energy lies at 112 kcal/mol.

Another difference between the fully quantal results and those of the classical Coulomb interaction model outlined above resides in the symmetry of the charge distribution in the former that is absent in the latter. Specifically, our quantal results show four equally charged H atoms, but in the above model, the classical Coulomb energy was calculated for a "charge localized" state. To further investigate the effects of charge delocalization, one can compute (e.g., at R(OH) = 1.0228 Å where all four O–H distances are equal) the Coulombic energy content of a unit positive charge on one H center with three +1/3 charges on the other three H centers compared to the Coulomb energy of four equal +1/2 charges on the four H centers. The former lies 196 kcal/mol above the $H_3O^+ + H^+$ asymptote, and the latter lies even 33 kcal/mol *higher*.

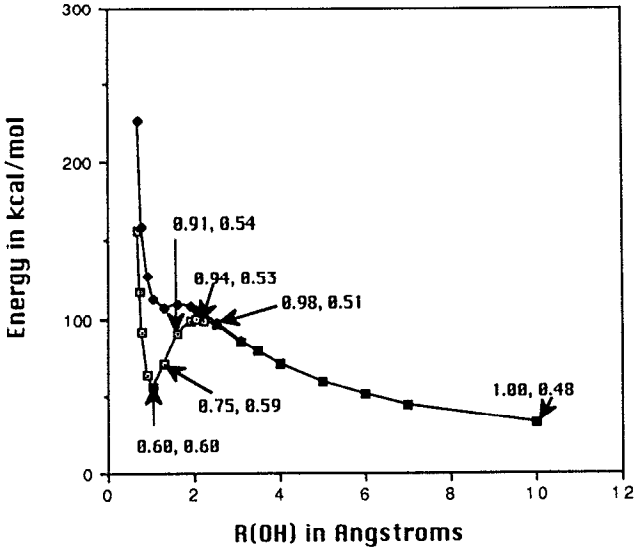

FIG. 1. The lowest energy curve gives a plot of the SCF/6–31G** ground state electronic energy (including nuclear repulsion) of H_4O^{2+} as a function of *one* O–H bond length R(OH) with the remaining internal coordinates of the H_3O moiety optimized to produce minimum energy for each value of R(OH). The partial charges on the departing H atom and those on the three remaining H atoms are given by the pairs of numbers (e.g., 0.94 and 0.53 are the charges near the barrier top). The higher energy curve represents the interaction energy of a single unit positive charge on the unique H atom center at R(OH) interacting with H_3O^+. The two curves are close or indistinguishable for R(OH) > $\sim$2.1 Å.

It may be surprising that four equivalent charges of magnitude 1/2 produce *greater* classical Coulombic repulsion energy than the charge localized state with one unit charge and three charges of magnitude 1/3. At first glance, this aspect of the classical model seems inconsistent with the results of our quantum calculations which show equal charge densities (i.e., average charges) on the four equivalent H atoms. To achieve any sense of agreement, one can postulate that four equally weighted classical "resonance structures" (each with one of the H atoms carrying $\sim$ unit charge and the remaining three having charge $\sim$1/3) are superposed to produce the quantum state and that the classical picture corresponds to only one of these resonance structures. The difference between the quantum and classical results is then ascribed to quantum interferences among the four structures.

3. High energy content of multiprotonated species

Of course, the T_d H_4O^{2+} and H_4S^{2+} structures are *not* the lowest-energy geometries that these species can realize. The dissociation products H_3X^+ and H^+ are predicted to be lower in energy by 61 and 91 kcal/mol, respectively, at the QCISD(T)/6–311(2*df*,2*p*)//MP2(full)/TZP+ZPE/MP2(full)/6–31G** level for these two dications. These T_d forms of H_4O^{2+} and H_4S^{2+} are separated from their dissociation products by barriers of 38 and 20 kcal/mol, as a result of which both of them may be sufficiently long lived to be detected in gas-phase experiments.

B. H_3F^{2+} and H_3Cl^{2+}

C_{3v} pyramidal structures with one lone electron pair on the central atom are expected (in analogy[14,15] with NH_3 and H_3O^+) for H_3F^{2+} and H_3Cl^{2+}. Both of these dications are found to have such local minima, but H_3F^{2+} actually has a D_{3h} planar structure (because the Coulomb repulsions between its hydrogen atoms are larger than in ClH_3^{2+}, which is found to have a pyramidal C_{3v} structure). At our highest QCISD(T)/6–311G(2*df*,2*p*)/MP2(full)/TZP+ZPE/MP2(full)/6–31G** level, the H_3Cl^{2+} dication has a high (18 kcal/mol) inversion barrier. However, this value is much lower than inversion barriers of the isoelectronic PH_3 [35 kcal/mol (Ref. 16)] and SH_3^+ [32 kcal/mol (Ref. 17)] species, again due to the larger Coulomb repulsion among the hydrogen centers of ClH_3^{2+}.

The H_3F^{2+} and H_3Cl^{2+} dications are predicted to lie above their dissociation products (H_2X^+ and H^+) by 111 and 67 kcal/mol, respectively, at the QCISD(T)/6–311G(2*df*,2*p*)/MP2(full)/TZP+ZPE/MP2(full)/6–31G** level. At this same level, our calculations indicate that H_3F^{2+} and H_3Cl^{2+} have 12 and 34 kcal/mol dissociation potential barriers, respectively.

C. H_2Ne^{2+} and H_2Ar^{2+}

For H_2Ne^{2+}, geometry optimization within $D_{\infty h}$ or C_{2v} symmetry leads to dissociation into $H^+ + Ne + H^+$. Hence, this dication has no local minimum on its ground-state potential energy surface. In contrast, the H_2Ar^{2+} dication is found to possess a local minimum which lies 116 kcal/mol above HAr^+ and H^+. However, this H_2Ar^{2+} structure is separated by a small barrier 5 kcal/mol from its dissociation products [all of this data refers to the QCISD(T)/6–311G(2*d*,2*p*)//MP2(full)/TZP+ZPE/MP2(full)/6–31G** treatment), and thus may have a short life time.

D. H_4F^{3+} and H_4Cl^{3+}

Both H_4F^{3+} and H_4Cl^{3+} are expected to have tetrahedral structures. However, H_4F^{3+} is found to possess three imaginary vibrational frequencies in T_d symmetry and to not possess a local minimum on its ground state potential energy surface. In contrast, H_4Cl^{3+} has a local minimum with no imaginary frequencies at tetrahedral symmetry, but the corresponding potential barrier on the dissociation pathway is very small and is exceeded by the ZPE correction. Therefore, both of these trications are predicted to be unstable. The fact that H_4Cl^{3+} is nearly stable suggests that H_4I^{3+} may be stable since the larger I atom should delocalize the 3+ charges over larger H-to-H distances.

E. H_3Ne^{3+} and H_3Ar^{3+}

For both of these species, geometry optimization within C_{3v} or D_{3h} symmetry [at the SCF/6–31G** and MP2(full)/6–31G** levels] leads to dissociation into Ne (or Ar) $+3H^+$ without any barrier, as a result of which both of these species are not viable.

F. H_4Ne4+ and H_4Ar^{4+}

These species also have no local minima on their respective potential energy surfaces because geometry optimization in T_d symmetry [at the SCF/6–31G** and MP2(full)/6–31G** levels] leads to dissociation into Ne (or Ar) $+4H^+$ without any barrier.

G. Energy content of the dications and mechanisms for its release

The multiply protonated cations studied in this paper possess a great deal of pent up energy as shown clearly in Fig. 1 and Table IV. If the barrier to dissociation can be surmounted (e.g., thermally), this energy may be released. The amount of energy released in such events is given as E_{diss} in Table IV, and ranges from ~60 kcal/mol to greater than 110 kcal/mol.

Alternatively, energy release can be achieved by reducing the parent species' charge state by one unit (e.g., electrochemically or by photoinduced electron transfer from a neighboring moiety). For example, as illustrated in Fig. 2, addition of a single electron to H_4O^{2+} to form H_4O^+ at the equilibrium geometry of the dication produces a very unstable situation. The nascent reduced species, which as Table VI shows vertically lies ~13 eV below the H_4O^{2+} dication, spontaneously dissociates to form $H + H_3O^+$ with a very large release of kinetic energy (over 90 kcal/mol of energy in the H_4O^+ case—see Fig. 2).

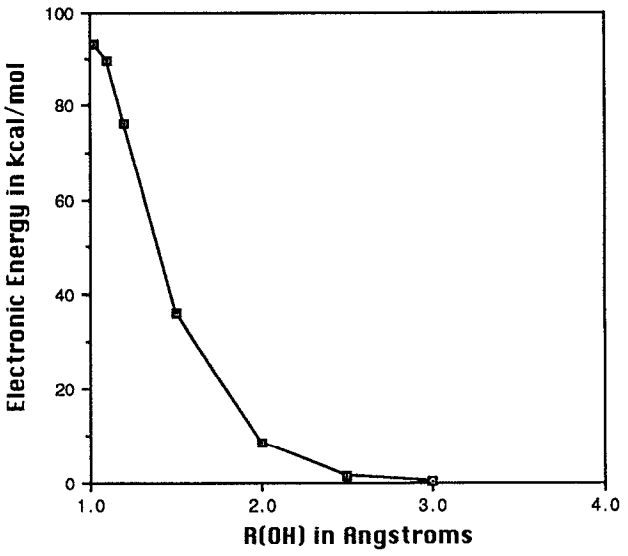

FIG. 2. Plot of the SCF/6–31G** ground state electronic energy (including nuclear repulsion) of H_4O^+ as a function of *one* O–H bond length R(OH) with the remaining internal coordinates of the H_3O moiety optimized to produce minimum energy for each value of R(OH). Note that the geometry corresponding to $R(\text{OH}) = 1.0228$ Å corresponds to the H_4O^+ that would be formed by attaching an electron to H_4O^{2+} at its equilibrium geometry.

The energy releases corresponding to the doubly charged cations studied here are detailed quantitatively in Tables IV and VI. In the former, energy differences appropriate to tunneling through or surmounting the barrier on the parent ion surface are given as E_{diss}. In the latter, the adiabatic energy differences, denoted ΔE_{ad}, *combine* the *electronic* energy gained by simply adding an electron to the parent species' at its equilibrium geometry (i.e., the vertical energy difference denoted ΔE_v in this table)

$$H_nM^{k+} + e \rightarrow H_nM^{(k-1)+} \quad (\Delta E_v)$$

and the subsequent kinetic energy released

$$H_nM^{(k-1)+} \rightarrow H + H_{(n-1)}M^{(k-1)+} \quad (\Delta E_{\text{diss}})$$

when the reduced species explodes. The explosion energies

$$\Delta E_{\text{diss}} = |\Delta E_{\text{ad}} - \Delta E_v|$$

inferred from the data of Table VI lie between 2.8 and 3.4 eV, or 64 and 78 kcal/mol. We note that the vertical attachment energies ΔE_v of the dications listed are in line with those of Be^{2+}, Mg^{2+}, Al^{2+}, Ni^{2+}, Cu^{2+}, and Zn^{2+}, which range from −15 to −20 eV.

IV. CONCLUSIONS

(1) The *doubly charged* H_4O^{2+}, H_4S^{2+}, H_3F^{2+}, H_3Cl^{2+}, and H_2Ar^{2+} cations are predicted to be metastable species that are not stable thermodynamically with re-

TABLE VI. Vertical (ΔE_v) and adiabatic (ΔE_{ad}) electron attachment energies in eV for doubly protonated species [within the 6–3111G(2*df*,2*p*) basis].[a,b]

	Reaction	SCF	PMP2	PMP3	PMP4
ΔE_v	$H_4O^{2+}+e \rightarrow H_4O^+$	12.4	13.1	13.1	13.2
ΔE_{ad}	$H_4O^{2+}+e \rightarrow H_3O^+ + H$	16.1	16.0	16.0	16.0
ΔE_v	$H_4S^{2+}+e \rightarrow H_4S^+$	13.2	13.9	13.9	14.0
ΔE_{ad}	$H_4S^{2+}+e \rightarrow H_3S^+ + H$	17.3	17.3	17.3	17.3
ΔE_v	$H_3F^{2+}+e \rightarrow H_3F^+$	14.7	15.4	15.4	15.4
ΔE_{ad}	$H_3F^{2+}+e \rightarrow H_2F^+ + H$	18.4	18.3	18.4	18.3
ΔE_v	$H_3Cl^{2+}+e \rightarrow H_3Cl^+$	12.9	13.3	13.3	13.3
ΔE_{ad}	$H_3Cl^{2+}+e \rightarrow H_2Cl^+ + H$	16.3	16.3	16.3	16.3
ΔE_v	$H_2Ar^{2+}+e \rightarrow H_2Ar^+$	14.7	15.1	15.1	15.1
ΔE_{ad}	$H_2Ar^{2+}+e \rightarrow HAr^+ + H$	18.6	18.6	18.5	18.5

[a]The vertical ΔE_v gives ΔE (ZPE corrected) for the process $H_nM^{k+} + e \rightarrow H_nM^{(k-1)+}$ at the geometry of H_nM^{k+}.

[b]The adiabatic ΔE_{ad} gives ΔE (ZPE corrected) for the combined process $H_nM^{k+} + e \rightarrow H_nM^{(k-1)+} \rightarrow H + H_{(n-1)}M^{(k-1)}$, in which $H_{(n-1)}M^{(k-1)}$ is produced at its optimal geometry.

spect to dissociation into $H_nX^+ + H^+$. All of these cations have local minima on their ground state potential energy surfaces with barriers that must be overcome to reach dissociation. The lifetimes of these multiply protonated species may be long enough to permit them to be experimentally observed.

(2) Because the above multiply protonated dications lie high above their respective dissociation products, and because the corresponding one-electron-reduced cations are geometrically unstable, a large amount of pent up energy can be released by adding a single electron (e.g., by charge transfer from a neighboring molecule or anion). These species thus may be good candidates for use in energy storage materials.

(3) The *triply charged* H_4F^{3+}, H_3Ne^{3+}, H_3Ar^{3+}, and *higher charged* H_4Ne^{4+}, H_4Ar^{4+} cations as well as the H_2Ne^{2+} dication do not possess local minima on their ground state surfaces. H_4Cl^{3+} has a local minimum on its potential energy surface, but its zero-point corrected energy lies slightly above its dissociation barrier.

ACKNOWLEDGMENTS

This work was supported in part by NSF Grant No. CHE9116286. We also thank the Utah Supercomputer Institute for staff and computer resources.

[1] S. G. Lias, J. F. Liebman, and R. D. Levin, J. Phys. Chem. Ref. Data **13**, 695 (1984).
[2] G. A. Olah, G. K. S. Prakash, M. Barzaghi, K. Lammertsma, P. v. R. Schleyer, and J. A. Pople, J. Am. Chem. Soc. **108**, 1032 (1986).
[3] G. A. Olah, G. K. S. Prakash, M. Marcelli, and K. Lammerstma, J. Phys. Chem. **92**, 878 (1988).
[4] C. Kozmutza, E. Kapuy, M. A. Robb, R. Daudel, and I. G. Csizmadia. J. Comput. Chem. **3**, 14 (1982).
[5] S. C. Choi, R. J. Boyd, and O. Knop, Can. J. Chem. **66**, 2465 (1988).
[6] H. B. Schlegel, J. Comput. Chem. **3**, 214 (1982).
[7] P. C. Hariharan and J. A. Pople, Theor. Chim. Acta **28**, 213 (1973).
[8] M. J. Frisch, J. A. Pople and J. S. Binkley, J. Chem. Phys. **80**, 3265 (1984).
[9] T. H. Dunning, Jr., J. Chem. Phys. **55**, 716 (1971).
[10] A. D. McLean and G. S. Chandler, J. Chem. Phys. **72**, 5639 (1980).
[11] R. Krishnan and J. A. Pople, Int. J. Quant. Chem. **14**, 91 (1978).
[12] J. A. Pople, M. Head-Gordon, and K. Raghavachari, J. Chem. Phys. **87**, 5958 (1987).
[13] GAUSSIAN 90. M. J. Frisch, M. Head-Gordon, G. W. Trucks, J. B. Foresman, H. B. Schlegel, K. Raghavachari, M. A. Robb, J. S. Binkley, C. Gonzalez, D. J. DeFrees, D. J. Fox, R. A. Whiteside, R. Seeger, C. F. Melius, J. Baker, R. L. Martin, L. R. Kahn, J. J. P. Stewart, S. Topiol, and J. A. Pople (Gaussian Inc., Pittsburgh, 1990).
[14] V. Spirko, J. Mol. Spectrosc. **21**, 3 (1983).
[15] T. J. Sears, P. R. Bunker, P. B. Davies, S. A. Johnson, and V. Spirko, J. Chem. Phys. **83**, 2676 (1985).
[16] R. Ahlrichs, F. Keil, H. Lischka, W. Kutzelnigg, and V. Staemmler, J. Chem. Phys. **63**, 455 (1975).
[17] D. A. Dixon and D. S. Marynick, J. Chem. Phys. **71**, 2860 (1979).